HHS Public Access

Author manuscript

J Vis. Author manuscript; available in PMC 2020 July 14.

Published in final edited form as:

J Vis. ; 8(14): 17.1–1714. doi:10.1167/8.14.17.

NIMBLE: A kernel density model of saccade-based visual memory

Luke Barrington,
Department of Electrical and Computer Engineering, University of California, San Diego, La Jolla, CA, USA

Tim K. Marks,
Department of Computer Science and Engineering, University of California, San Diego, La Jolla, CA, USA

Janet Hui-wen Hsiao,
Department of Computer Science and Engineering, University of California, San Diego, La Jolla, CA, USA

Garrison W. Cottrell
Department of Computer Science and Engineering, University of California, San Diego, La Jolla, CA, USA

Abstract

We present a Bayesian version of J. Lacroix, J. Murre, and E. Postma's (2006) Natural Input Memory (NIM) model of saccadic visual memory. Our model, which we call NIMBLE (NIM with Bayesian Likelihood Estimation), uses a cognitively plausible image sampling technique that provides a foveated representation of image patches. We conceive of these memorized image fragments as samples from image class distributions and model the memory of these fragments using kernel density estimation. Using these models, we derive class-conditional probabilities of new image fragments and combine individual fragment probabilities to classify images. Our Bayesian formulation of the model extends easily to handle multi-class problems. We validate our model by demonstrating human levels of performance on a face recognition memory task and high accuracy on multi-category face and object identification. We also use NIMBLE to examine the change in beliefs as more fixations are taken from an image. Using fixation data collected from human subjects, we directly compare the performance of NIMBLE's memory component to human performance, demonstrating that using human fixation locations allows NIMBLE to recognize familiar faces with only a single fixation.

Keywords

computational modeling; eye movements; face recognition; object recognition; memory; kernel density estimation

Corresponding author: Gary Cottrell. gary@ucsd.edu. Department of Computer Science and Engineering 0404, University of California, San Diego, La Jolla, CA 92093-0404, USA.

Commercial relationships: none.

Introduction

In human visual perception, we repeatedly foveate different areas of a visual scene, concentrating fixations on the parts that are most salient or task-relevant (Yarbus, 1967). It is still mysterious how we nevertheless are able to recognize objects from these samples. It would be slightly less mysterious if we fixated exactly the same locations each time we viewed an image and thus extracted identical fragments. However, while the scan paths we use may be similar between two observations of the same image (Foulsham & Underwood, 2008), it is by no means a requirement for high recognition rates that we fixate the same locations (Henderson, Williams, & Falk, 2005). For example, Henderson et al. (2005) showed that subjects do not make significantly different fixations during face recognition compared to control subjects after having their fixations artificially restricted during face learning. In other words, the scan paths generated during recognition may not be just replicating those followed during learning, as proposed by the scan path theory of Noton and Stark (1971). Thus, simple exemplar matching of information from new saccades to stored memories cannot be relied upon to account for human capacities for object recognition, as the exemplars may differ between study and test.

Lacroix, Murre, Postma, and Van den Herik (2004) and Lacroix, Murre, and Postma (2006) have proposed the Natural Input Memory (NIM) model to account for humans' ability to recognize faces from fixations. (We use the term face *recognition* in the sense used in the experimental psychology literature. It refers to the ability to discriminate previously seen faces from novel faces, based on a study list. In contrast, we use face *identification* to refer to the ability to identify face images as particular individuals). NIM is an exemplar model of memory (Raaijmakers & Shiffrin, 2002), in that it stores memories as points in a vector space and compares memories based on distances in this space. However, NIM differs from standard mathematical psychology models in that (a) it uses actual facial images as input and (b) it is based on the idea of storing fixation-based face fragments, rather than whole face exemplars. The NIM model's memory is reminiscent of a kernel density estimator but differs in important details from a true probabilistic model in the way that the estimates from individual fragments are combined. In this paper, we present a Bayesian version of the NIM model that uses naive Bayes to combine the likelihood estimates from individual fragments. We further extend the model to perform multi-class visual memory tasks and to use a variety of kernels for density estimation. Our model, which we call NIMBLE (for NIM with Bayesian Likelihood Estimation), achieves human levels of performance on a standard face recognition task and also performs multi-class face and object identification tasks with high accuracy. Bayesian combination of individual fragment likelihoods outperforms the combination method from the original NIM model in most cases, and the new kernels far outperform those used in NIM.

Though there are few cognitive models of saccade-based visual memory, fragment-based models are common in computer vision. Supporting the idea that the whole image can be recovered from sampling only at interesting fixation points, the work of Raj, Geisler, Frazor, and Bovik (2005) on entropy minimization of natural scenes demonstrates that images can be reconstructed from fragments. Ullman, Vidal-Naquet, and Sali (2002) used the mutual

information between an image fragment and the class label of the object from which it is sampled to show that fragments of intermediate complexity (fragments that are smaller than the total object but much larger than a pixel) are most useful for image classification. The SIFT features proposed by Lowe (2004) are based on finding key points in images that are invariant to changes of scale, orientation, and illumination, then describing each point using histograms of image gradients in the region surrounding the point. Belongie, Malik, and Puzicha (2002) find interest points in images and model the correspondence between the shapes described by these points to compare and classify images. Applying fragment-based representation to video, Dollar, Rabaud, Cottrell, and Belongie (2005) find interest points in three-dimensional video signals and extract spatio-temporal fragments (called cuboids) for use in behavior classification. Thus, not only are image fragments a biologically plausible representation for image classification, they have also been used quite successfully in computer vision applications.

In the Methods section, we begin by describing our biologically motivated image sampling and transformation procedure. We then describe the NIM model. Next, we explain our Bayesian version of the model, NIMBLE, including a variety of extensions. We compare human and model performance on visual memory tasks in the Results section, and conclude the paper with a discussion.

Methods

Visual input simulation

Fixation point selection—Given a current fixation point, the choice of where to saccade to next is driven by a number of external cues including motion, peripheral complexity, and non-visual stimuli (such as sound), as well as top-down task-dependent directives such as attention and expectation. Though many computer models (e.g., Mozer, Shettel, & Vecera, 2006; Wolfe, 1994; Zelinsky, Zhang, Yu, Chen, & Samaras, 2006) have been proposed for how to integrate top-down and bottom-up cues, in this work we select fixations based only on the bottom-up salience of static images. We model the fixation selection process using a local interest operator for determining the scan paths (Yamada & Cottrell, 1995). This model uses the rotational variance of eight low-resolution Gabor filter responses to construct a distribution of the contour complexity (salience) over all pixels in a given image:

$$\text{Salience}(i,j) = \frac{1}{8}\sum_{n=1}^{8}\left(G(i,j,\theta) - \mu_G(i,j)\right)^2, \quad (1)$$

where $G(i, j, \theta)$ is the magnitude response of a Gabor filter with orientation θ centered at pixel (i, j), and $\mu_G(i, j)$ is the mean response across all eight orientations. A similar technique developed by Renninger, Coughlan, Verghese, and Malik (2005) defines salience as the entropy, rather than the variance, of local image contours.

We convert this salience map into a probability distribution using the softmax function (Bishop, 1995). A fixation point is then chosen randomly according to this distribution. Figure 1 shows a salience map generated in this manner as well as a sample distribution of fixation points. After each fixation point is chosen, we reduce the salience around the fixated

point by subtracting from the salience distribution a rotationally symmetric Gaussian, centered at the fixation point, and then renormalizing. This inhibits repeated fixations of the same location and prevents fixations from clustering in areas that are initially highly salient. A given image will always have the same initial salience map, but by randomly sampling from this distribution and inhibiting return to fixated locations, repeated viewings of the same image will result in different scan paths.

Despite the simplicity of this purely bottom-up model, the resulting scan paths for the face recognition task qualitatively approximate those observed in humans (Yamada & Cottrell, 1995). The model satisfies three of the five criteria identified by Itti and Koch (2001) for a computational model of visual attention: it derives perceptual salience of a fixation point from the surrounding context, it creates a salience distribution over the visual scene, and it inhibits return to previously attended locations. In this paper, we ignore the remaining two criteria, which concern top-down influences on fixation point selection. Since this salience model is fully probabilistic, it could be combined with top-down feedback to direct eye movements, for example, by extending the results of Nelson and Cottrell (2007) to determine the fixations that would be most useful in enhancing performance on the current visual task.

We have tested NIMBLE using various alternative mechanisms for computing visual salience (for selecting fixations). NIMBLE using the salience operator of Itti and Koch (2001) results in roughly the same face recognition performance as NIMBLE using the salience operator (Equation 1) of Yamada and Cottrell (1995), but the latter approach has the advantage that the same mechanism (Gabor filters) is used for computing salience as for processing images (see the Retinal/cortical image transform section). Purely random selection of fixations (corresponding to a uniform salience map) reduces performance by 30%. Sampling fixations from the Canny edge map of the image, as was done in the NIM model, reduces performance by 20%. We also tested NIMBLE using the locations of actual human fixations, which were recorded from the same face images using an eye tracker (Hsiao & Cottrell, in press). A detailed description of this experiment is given in the Results section.

Retinal/cortical image transform—A fixated patch of an input image undergoes many stages of neural processing before being represented as a pattern of activation in high-level visual cortex. Our biologically inspired model of the processing in primary visual cortex (V1) uses the magnitude responses of Gabor filters at 8 orientations and 4 frequencies (Jones & Palmer, 1987). At each orientation, we use Gabor filter frequencies of $\frac{1}{16}$, $\frac{1}{12}$, $\frac{1}{8}$ and $\frac{1}{4}$ cycles/pixel (corresponding to 8, $10\frac{2}{3}$, 16, and 32 cycles/face) to approximate the varying resolution available to the retina. We transform an image into the Gabor-filtered domain by calculating the response of each of these 32 filters (8 orientations × 4 frequencies) at every image pixel.

The model approximates a foveated representation of the fixated location by extracting square patches from these Gabor response images. The highest spatial frequency filter responses correspond to the high-resolution foveated area centered at the fixated location.

The low-frequency filter responses at a given pixel within the square patch are computed from an image area with spatial context that extends beyond the borders of the patch—a low-resolution filter placed at the edge of a patch responds with one quarter of its peak magnitude at 52 pixels from the fixation point or 40% of the width of the test images, corresponding to a visual angle of 3.2° (assuming a real face viewed from a distance of 1 m occupies 8° of the visual field; Henderson et al., 2005). Thus, this patch-based representation includes extrafoveal information corresponding to the low-resolution data from the retinal periphery.

The size of the extracted patch of filter responses and the number of fragments that the model may examine for each image are experimental parameters that correspond, in human vision, to the distance of the eye from the image (and thus the size of the foveated area) and the time spent studying the image (determining the number of fixations made). For a fragment size of 35 × 35 pixels (corresponding to a visual angle of 2° for a subject about 1 m from a real face, an approximation of the human studies discussed below), the model's input feature vector has 35 × 35 pixels × 8 orientations × 4 frequencies = 39,200 dimensions. This fragment size was chosen to approximate the experimental conditions experienced by the human subjects whose data we model in the NIMBLE using human fixations section, but the NIMBLE model could use image fragments of any size. For efficiency and good generalization, we use principal component analysis (PCA) to reduce the size of this vector to 80 components, retaining about 90% of the data variance (depending on the data set—see the Results section). This feature extraction procedure of wavelet-based image decomposition followed by PCA is a standard approximation for biologically motivated vision models (Dailey, Cottrell, Padgett, & Adolphs, 2002; Lacroix et al., 2006; Palmeri & Gauthier, 2004).

The Natural Input Memory (NIM) model

The inspiration for our model of saccade-based vision comes from the work of Lacroix et al. (2004, 2006). Their Natural Input Memory (NIM) model is so called since it takes biologically inspired saccade-like samples from a studied image as input. Their sampling method differs slightly from ours in that they sample from the contours of an image, determined by Canny edge detection, and then process the sampled patches with the steerable pyramid transform, a multi-scale wavelet-based transform that is similar to Gabor filtering. They then apply PCA to these features before storage in the memory.

Following the lead of many cognitive memory models (Dailey, Cottrell, & Busey, 1998; Hintzman, 1984; Nosofsky & Palmeri, 1997), the NIM model's memory process stores the feature-transformed representation of fixated image fragments as vectors in a high-dimensional memory space. Memories are compared to each other as well as to new image fragments by comparing the Euclidean distance between their vector representations in this memory space. The NIM model computes the familiarity of a new fragment by calculating the proportion of previously stored memories that lie within a radius r (a model parameter) of the new fragment in the memory space. Averaging these familiarities over all samples from a new image produces an estimate of the probability that the image is from the class known to the memory. The memory space introduced by the NIM model has been shown to

achieve the best known correlation with human judgments of perceptual similarity (Lacroix et al., 2006), and the retrieval methods exhibit human performance effects (such as list length and list strength) on face recognition memory tasks (Lacroix et al., 2004).

The NIM memory retrieval method (Lacroix et al., 2006) determines the familiarity of a newly examined fragment by counting how many of the stored memories, $\{m_1, \ldots, m_M\}$, lie within a radius r of the new image fragment. Thus, the familiarity of the new fragment, f, is defined by

$$\mathrm{fam}(f) = \sum_{j=1}^{M} I_r\left(\|m_j - f\|_2\right), \tag{2}$$

where

$$I_r(x) = \begin{cases} 1, & x \le r \\ 0, & \text{otherwise.} \end{cases} \tag{3}$$

NIM combination of fragment familiarities—An image is represented as a set of N fragments $F = \{f_1, \ldots, f_N\}$. In the NIM model, Lacroix et al. (2006) define the familiarity of a test image as the mean of the familiarities of all N fragments taken from that image:

$$\mathrm{fam}(F) = \frac{1}{N} \sum_{i=1}^{N} \mathrm{fam}(f_i)\,. \tag{4}$$

They use a logistic function to transform this mean familiarity value into a probability value between 0 and 1:

$$P(\text{familiar image}) = \frac{1}{1 + \beta e^{-\theta \mathrm{fam}(F)}}, \tag{5}$$

where β and θ are parameters of the model used to fit the performance to human data.

The NIM model formulation (Lacroix et al., 2006) only attempts to make judgments about the familiarity of a studied image by comparing a set of fragments extracted from the image to all previously stored memories. Since these memories are stored without labels, the resulting familiarity value must be compared to a threshold to decide whether the image is familiar or unfamiliar. Our extension of NIM, described in the A more NIMBLE approach section, stores class labels with each exemplar and can return explicit posterior probabilities for each class given the image fragments, permitting multi-class and hierarchical memory tasks in addition to the familiar/unfamiliar recognition memory task of Lacroix et al. (2006). More recent versions of NIM (e.g., NIMCLASS (Lacroix, Postma, & Van den Herik, 2007) have also been extended to classification. These more recent versions are compared to our model in the Discussion section.

A more NIMBLE approach

Having sampled and processed a new image as described above in the Retinal/cortical image transform section, we want to evaluate the probability of the resulting set of N fragments, $F = \{f_1, \ldots, f_N\}$, under the models for each of a number of image classes. For instance, we handle the previously described familiar/unfamiliar faces task as a two-class problem and can additionally handle other classification tasks such as Alice/Bob/Carol/Dan/unknown or dogs/not dogs. For each class, c, we use Bayes rule to compute the posterior distribution:

$$p(c \mid F) = \frac{p(F \mid c)p(c)}{p(F)}. \tag{6}$$

In this case, $p(F|c)$ is the likelihood of the set of image fragments under the density model for class c, and $p(c)$ is the class prior which may be learned from experience with training data.

We compute the likelihood of the set of image fragments, $p(F|c)$, by combining the likelihoods of each individual fragment, $p(f_i|c)$, as explained in the Naive Bayes fragment combination section. Each of these class-conditional fragment likelihoods is computed using kernel density estimation (see the Kernel density estimation section).

Naive Bayes fragment combination—In the NIMBLE model, we make the naive Bayes assumption of conditional independence between each fragment $f_i \in F$, given the class, and take the product of the individual fragment likelihoods to obtain an estimate of the overall likelihood function:

$$p(F \mid c) = \prod_{i=1}^{N} p(f_i \mid c). \tag{7}$$

By integrating fragment likelihoods using the naive Bayes combination (Equation 7), we can obtain a parameter-free estimate of the posterior probability of each class given the image.

In contrast, if we conceive of the familiarity of image patches in the NIM model as fragment likelihoods, then we can think of NIM's fragment integration method (Equation 4) as defining the likelihood of an image to be the mean of its fragment likelihoods:

$$p(F \mid c) = \frac{1}{N} \sum_{i=1}^{N} p(f_i \mid c). \tag{8}$$

Combining fragment likelihoods by taking their product using the naive Bayes method (Equation 7) assumes that the probabilities of observing each patch are conditionally independent, given the class. While this assumption is clearly not true (e.g., if our first glimpse of a picture of a randomly chosen friend reveals Alice's left eye, it is very likely that a further saccade will reveal Alice's right eye), explicitly modeling the class-conditional dependencies of all possible sets of observable fragments is computationally intractable. While it is unwarranted, at least the conditional independence assumption is explicit in the model, and this probabilistic framework allows for the inclusion of higher level

dependencies. In contrast, the probabilistic interpretation of the implicit assumptions about dependence between fragments in the mean familiarity method of combination (Equation 4) is unclear, though Kittler, Hatef, Duin, and Matas (1998) have indicated that such ad hoc methods can perform well in practice.

Bayesian classification—The classification decision is made by comparing the log ratio of the class and non-class posteriors:

$$\log\frac{p(c\,|\,F)}{p(\bar{c}\,|\,F)} = \log\frac{p(F\,|\,c)p(c)}{p(F\,|\,\bar{c})p(\bar{c})} = \log\frac{p(F\,|\,c)}{p(F\,|\,\bar{c})} + \log\frac{p(c)}{p(\bar{c})}. \tag{9}$$

The first term on the right-hand side of Equation 9 compares the relative likelihoods of the observed fragments under the class and non-class models. The second term controls the bias or prior weight that the model or subject puts on seeing images from class c versus all other images. The Bayes decision rule classifies the image as coming from class c when Equation 9 is positive and from class $\bar{c}$ otherwise. In the multi-class framework, the Bayes-optimal rule is to choose the class with the largest posterior probability:

$$c^* = \underset{c}{\operatorname{argmax}}\ p(c\,|\,F). \tag{10}$$

Kernel density estimation—Kernel density estimation centers a kernel function at the point in memory space corresponding to every memorized fragment and computes the probability density of a new point (new fragment) f under each of these kernels. The sum of these probabilities forms the overall estimate of the likelihood of the new fragment, $p(f|c)$. The choice of kernel function and the parameters that control its shape are design features of the model, which we will consider below.

We may interpret the original NIM (Lacroix et al., 2006) measure of a new fragment's familiarity (Equation 2) as a kernel density estimate that centers a hypersphere of radius r, with uniform density, at the location of each stored exemplar in memory space. The familiarity of a new fragment, f, can be viewed as summing its density under all of these uniform kernels. By casting the problem of memory retrieval as a kernel density estimation task, we can explore the model's performance under a variety of kernel functions beyond the hypersphere in Equation 2. Indeed, this NIM kernel prohibits using the naive Bayes combination of fragment likelihoods (Equation 7), since if a test fragment f were to find no stored points within radius r, it would be assigned zero likelihood. In that case, even if all other fragments were strongly predictive of the class, the resulting product of fragment likelihoods would be $p(F|c) = 0$.

We have implemented the NIMBLE model using two alternative kernel functions. The first is a Gaussian kernel:

$$p(f \mid c) = \frac{1}{|M_c|} \sum_{j=1}^{|M_c|} N(x, \mu, \sigma), \tag{11}$$

where $N(x, \mu, \sigma)$ represents the normal probability density function of x with mean μ and variance σ, and $M_c = \{m_1, m_2, \ldots, m_{|Mc|}\}$ is the set of previously memorized fragments from class c. The second is a k-nearest-neighbor (kNN) kernel:

$$p(f \mid c) \propto \frac{k_c}{|M_c|V}, \tag{12}$$

where V is the minimum volume centered at f that contains k stored memories, of which k_c are from class c (Bishop, 1995).

NIMBLE's Bayesian framework can accommodate both naive Bayes combination of fragment likelihoods (Equation 7) and NIM's averaging method of combining fragment likelihoods (Equation 8). In Tables 1 and 2, we refer to these two methods for obtaining an overall image likelihood from fragment likelihoods as *Naive Bayes* and *Mean familiarity,* respectively. In each table, we also indicate the best parameter setting (value of σ or k) for each kernel, where optimization over the parameters was performed using 10 random trials.

Results

In this section, we present the results of applying NIMBLE to a face identification task, an object identification task, and a face recognition (memory) task.

Experimental data

In the experiments described below, we consider both face and object data sets. For facial identity and memory tasks, we use as input 128 × 192 pixel grayscale images from the FERET database (Phillips, Wechsler, Huang, & Rauss, 1998). Images of male and female Caucasian faces without facial hair or glasses were chosen, and the images were centered and normalized to have common eye positions and equal contrast. An example may be seen in Figure 1a. For object identification tasks, we use 128 × 128 pixel grayscale images of 20 objects from the COIL-100 data set (Nene, Nayar, & Murase, 1996).

Multi-class face and object identification

Since the NIMBLE model allows memories to be stored with class labels, unlike the original NIM model (but like other NIM extensions such as NIM-CLASS; Lacroix et al., 2007), we can apply NIMBLE to multi-class identification tasks. In this paradigm, the model is trained using $N = 10$ fragments to represent 3 images (with different lighting, expressions, or orientations) from 29 different FERET face identities or 20 COIL-100 object classes and tested on 3 unseen images from each of these classes. In this *identification* task, the model is presented with a novel test image that it has never seen before, and it must identify which category this novel image belongs to, based on previously studied images from the same face or object category. This is unlike the face *recognition* task described below in which the model must recognize the exact face images that it has previously studied.

For each test image, the output of the model is the posterior probability for each class, and the classification decision is made using Equation 10. For this multi-class problem, we assign equal prior probability to each of the classes and evaluate overall performance as the average accuracy across all classes. Note that the optimal parameter, σ, for the Gaussian kernel depends on the class of images to be identified since the within-class variance of patches taken from rotating objects (COIL-100) is much higher than the variance across patches sampled from aligned faces (FERET). We fit this parameter by 10-fold cross validation on randomly sampled image sets. Identification task results are shown in Table 1. Our model demonstrates high performance on these multi-class tasks. For example, our best object recognition model (kNN with Naive Bayes) achieves a respectable performance of almost 93%. A state-of-the-art computer vision system for object recognition, Belongie's shape context system (Belongie et al., 2002), achieves 97.6% accuracy on the same task. However, that system uses far more complex— and less biologically plausible—methods for selecting and matching correspondence points.

We use this multi-class task to demonstrate the advantage of using the naive Bayes method for combination of fragment likelihoods (Equation 7) over the mean familiarity method (Equation 8) used by Lacroix et al. (2006). For certain images, a given fragment may be either diagnostic of its true class or useful in excluding another class. In both cases, simply adding this fragment's likelihood to a running average over fragments (Equation 8) provides less useful modification to the ultimate posterior than does the naive Bayes updating method of multiplication (Equation 7). This is illustrated in Figure 2, which plots the mean posterior probability of the correct class in the facial identification task, averaged over all 29 facial identities. For this figure, we use an online version of NIMBLE to update the posterior, $p(c|F)$, as each fragment is added to F. With more information, the posterior for the correct class using naive Bayes likelihood combination (Equation 7) rises toward 1, while the posterior calculated using mean familiarity (Equation 8) remains roughly constant. The posterior probabilities of the 28 incorrect classes are not shown, but since the sum over all 29 classes must equal unity, it is clear that each incorrect class has very low probability, and therefore, the Bayes decision rule (Equation 9) almost always results in correct classification. For comparison, random guessing would set $p(c|F) = \frac{1}{29}$. Note that the results shown in Figure 2 reveal that, on average, a single fixation is enough to correctly identify a face.

Face recognition

Having validated NIMBLE's capabilities as a saccade-based face and object identification model, we now test it on a standard human memory task. We begin by testing NIMBLE's memory performance on a simple face recognition task. We follow the standard formulation of many human experiments, including Hsiao and Cottrell (in press), which we will examine further below. In the study phase (training phase) of our simulations, NIMBLE extracts N =10 fragments (approximating the number of saccades a human makes in 3 s) from each of 32 target images of faces. NIMBLE samples each of the 32 target faces and stores the resulting 320 fragments in the model's memory space. During the testing phase, NIMBLE extracts a new set of N fragments from 64 test face images, of which 32 are the original targets and 32 are novel distracters, known as lures. The model's task is to classify each image in the test phase as target (familiar) or lure (unfamiliar).

When viewing an image, NIMBLE selects a set of fixation points that are independent samples from the salience distribution for that image. Although the fixation points chosen during training and testing are sampled from the same underlying salience distribution, the stochasticity involved in this process, as well as the renormalization that results from the suppression of previously fixated locations, means that the actual fixation locations are almost always different. As Henderson et al. (2005) demonstrated, human scan paths in facial memory retrieval are not just replicating those generated during memory encoding, and so simple exemplar matching may not perform well. In our experiments, the mean distance from a point sampled from a face during encoding to the nearest point from the same face studied during retrieval was 8.8 pixels or 0.5 degrees of visual angle.

Since we do not restrict our model to discrete kernel functions such as Equation 2, in which only a subset of the stored memories contribute to the old/new decision, all stored memories from a given class contribute to the estimate of the posterior probability of the class. In order to apply the Bayes decision rule (Equation 9) to this one-class recognition task, we recast it as a two-class classification task. Fragments from training images are stored with a class label that indicates they have been seen in the study phase.

We need to estimate the likelihood that an image fragment was generated by the lure (distracter) class, $p(f|\bar{c})$. To estimate this probability, we use a multivariate Gaussian whose variance in each feature dimension is set equal to the principal component (eigenvalue) obtained by performing PCA on fragments extracted from 55 face images not used in the study or test phases. We used this method because it approximates storing a large number of face patches that a subject might see over her lifetime but is computationally faster than explicitly sampling from an extra set of non-task images. We compared the effect of using two different background models to estimate $p(f|\bar{c})$: a low-dimensional background model using the first 10 principal component dimensions and a high-dimensional background model using the first 80 principal component dimensions. In Table 2, we refer to these as 10-D BG and 80-D BG, respectively. The Gaussian kernel suffers a drop in performance when using the high-D background model because the extra dimensions of the 80-dimensional background model (which account for the least variance in the data) are quite susceptible to noise. When categorizing a new input, the kNN model (k =1) uses only one data point, unlike the Gaussian model which takes input from every point in memory. As a result, the kNN model is less affected by noise.

For each set of test fragments, we compute the posterior probability that these image fragments were generated by the target $p(c|F)$ and lure distributions $p(\bar{c}|F)$. Computing the (log) ratio of these probabilities (as in Equation 9) for each image provides a ranking of the images in order of how likely they are to be a familiar target image; larger values of $\frac{p(c|F)}{p(\bar{c}|F)}$ are more likely to be targets rather than lures. We quantify the model's results using the area under the receiver operating characteristic (ROC) curve. The ROC curve compares the rate of correct detections to false alarms at each point in the ranking. By varying the prior probabilities for each class, $p(c)$ and $p(\bar{c})$ (which comprise the second term on the right-hand side of Equation 9), we can trace out every point on the ROC curve and compute the area under the curve. This ROC area provides a single number that describes the accuracy of the

ranking (often estimated non-parametrically in psychophysics experiments as A'). For example, when $p(c) = 0$, all images are deemed to be lures, whereas when $p(\bar{c}) = 0$, all images are recognized as targets. A perfect ranking (i.e., all the target images at the top of the ranking and all the lures at the bottom) would result in an ROC area equal to 1. Ranking images randomly, we would expect the ROC area to be 0.5.

The results for the recognition memory task are shown in Table 2. We can see that in this task the mean familiarity model performs quite well. When tested on face images, normal human subjects achieved A' (a bias-free, nonparametric estimate of ROC area) in the range of 0.9 to 1.0 for this task (e.g., Duchaine & Nakayama, 2005; Hsiao & Cottrell, in press), and NIMBLE performs similarly. A more detailed analysis of NIMBLE's performance in comparison to humans is given in the NIMBLE using human fixations section.

NIMBLE using human fixations

The memory experiments described above demonstrate that NIMBLE performs well on standard memory tasks: NIMBLE approaches a more sophisticated computer vision model's object identification abilities, and NIMBLE recognizes familiar faces as well as humans. This performance arises in spite of NIMBLE's simple, bottom-up model of visual salience. In order to test the saccade-based memory component of the model in isolation (independent of the salience model), we examine NIMBLE's performance on a memory task for which we know the exact fixation locations used by humans.

Human face recognition with varying numbers of fixations—We conducted a human experiment to examine how many fixations are required to recognize a face (Hsiao & Cottrell, in press). During an otherwise standard face recognition task, participants were allowed a variable number of fixations (one, two, three, or no restriction/free viewing) before the stimulus was masked. The stimuli consisted of 16 male and 16 female Caucasian face images, taken from the FERET database (Phillips et al., 1998). During the experiment, the image size on the screen spanned about 8 degrees of visual angle, equivalent to the size of a real face at a viewing distance of 1 m; an area approximately the size of one eye on the face may be foveated at a time. The eye movements of eight male and eight female right-handed participants were recorded with an EyeLink II eye tracker. The tracking mode was pupil-only, with a sample rate of 500 Hz.

As in the NIMBLE face recognition experiments described above, the human experiments had a study phase and a test phase and used the same stimuli as the NIMBLE experiments. During the study phase, participants saw the 32 faces, one at a time, for 3 s in a random order. During the test phase, they saw the same 32 faces as well as 32 lures, one at a time. For each test stimulus, they were asked to judge, as quickly and accurately as possible, whether or not they had seen the face during the study phase by pressing "YES" or "NO" buttons within 3 s. The faces were divided into the four fixation restriction conditions evenly, counterbalanced through a Latin square design: one fixation, two fixations, three fixations, and no restriction (free viewing). In each trial, the image remained on the screen until either the participant's eyes moved away from the last permissible fixation (if a restriction was imposed), or the response occurred, or the end of 3 s, whichever came first.

The image was masked by the average face (an image created using the pixel-wise average of all of the stimuli from the study) after the last permissible fixation; the mask remained until the response or the end of 3 s. The participants were not informed of the association between the mask and the number of fixations they made during the experiment. One major difference from the NIMBLE experiments is that the human subjects had to saccade to the face after it appeared above or below a fixation point. Initially, the average face appeared, then during the subjects' first saccade it was replaced by the test face. This method was used to ensure that the subjects were unable to extract any identity information from peripheral vision. NIMBLE, on the other hand, is given the entire face to start with and computes salient points directly on the facial image.

Figure 3 shows the distribution of the first three fixations and overall fixations from all subjects during the study and the test phases. The participants' discrimination performance as measured by A', a bias-free nonparametric measure of sensitivity that estimates ROC area, showed that the optimal human recognition performance was achieved with two fixations—performance did not improve with additional fixations. This is illustrated in Figure 4: The A' in the two-fixation condition was significantly larger than that in the one-fixation condition ($F(1, 15) = 44.435$, $p < 0.001$); in contrast, A' in the two, three, and no restriction (4+ fixations) conditions were not significantly different from each other (there were no statistically significant differences between any two of the three).

NIMBLE face recognition using human fixations—In the human memory experiment just described (Hsiao & Cottrell, in press), we recorded the eye movements of 16 subjects as they performed both the study and test phases of a face recognition memory task. It is clear that the distribution of human fixations (Figure 3) differs significantly from the fixation locations chosen using NIMBLE's current model of visual salience (demonstrated in Figure 1). These differences most likely arise from two sources: 1) The human subjects start off the face and saccade to it, making the center of the face a more likely target; and 2) the simplified salience model (Equation 1) of Yamada and Cottrell (1995) takes no account of the top-down, task-specific cues used in directing human saccades. By using the human fixation locations recorded from the eye tracking experiment described above, rather than fixations drawn from a computed salience map, we can test the fragment memory component of NIMBLE in isolation from the salience model.

Using the same images and the same test paradigm as Hsiao and Cottrell (in press), we use the recorded human fixation locations as the basis for NIMBLE's fragment selection. During the study phase, we extract an image fragment from each of the locations where a human subject fixated a study image and store these fragments in NIMBLE's memory. During the test phase, we extract fragments from the locations in the target and lure images that subjects fixated during the test phase under each of the 4 fixation conditions and compute the likelihood of these fragments under NIMBLE's kernel density estimate of the target and lure classes. We calculate NIMBLE's ROC curves as before, this time using the fixation locations from each human subject, and compare the performance in each of the four fixation conditions. The results are shown in Figure 5, where we use a Gaussian kernel with $\sigma = 0.1$ to best fit the human data. (Note that the results for the original NIMBLE face recognition experiments in Table 2 are very insensitive to the value of this parameter, and

setting $\sigma = 0.1$ with the computed salience map provides similar results to those shown in Table 2.)

For comparison with Figure 4 (which shows human subjects' performance) and Figure 5 (which shows the performance of the NIMBLE model using actual human fixations), we have included Figure 6, which shows the NIMBLE model's performance using one, two, three, and the mean of four to ten fixations that were selected using the visual salience model (Equation 1) of Yamada and Cottrell (1995).

Figures 4 and 5 demonstrate that with limited fixations, NIMBLE using human fixations recognizes faces with similar accuracy to humans (with ROC area between 0.8 and 0.9). However, the two graphs also show that NIMBLE's trend in performance differs from humans. In particular, NIMBLE achieves maximum performance using just the first human fixation. Note that this is not the case when NIMBLE chooses fixations using the model of visual salience (Equation 1), as shown in Figure 6. This is consistent with the claim that the location chosen by humans for the first fixation (the bridge of the nose) may be the optimal viewing position for face recognition (Hsiao & Cottrell, in press).

A possible explanation for the discrepancy between the human results in Figure 4 and NIMBLE's performance using the same fixations in Figure 5 is that, as shown in Figure 3, the first and second fixations made by the human subjects tended to land in very similar locations (around the bridge of the nose), while it was not until the third fixation that attention was directed to the eyes. This suggests that all of the information required for face recognition in this task was obtainable by fixating the bridge of the nose, but that perhaps the subjects were not able to obtain all of the information required for face recognition during the duration of a typical fixation. Since we move our eyes about three times per second (Henderson, 2003; in the human experiment described above, the first fixation lasted 295 ms and the second fixation lasted 315 ms on average), it may be that a second fixation in a nearby location is required to accumulate more information and thus achieves the best face recognition performance. The need for a second fixation nearby the first may also be due to task switching from localizing to exploring for recognition. This task-switching effect could result from subjects planning a localizing saccade from the center of the screen to the target face stimulus before the first fixation; this localizing saccade has been shown to have a central bias (e.g., Renninger, Verghese, & Coughlan, 2007; Tatler, 2007). Obviously, the NIMBLE model does not experience this limitation.

While the performance on the second and third fixations are almost identical for human subjects and NIMBLE with human fixations, the performance of NIMBLE using human fixations degrades in the unrestricted viewing condition (4+ fixations, in which the model used up to 3 s of recorded human fixations on each image). This drop in performance may be because most human subjects had recorded enough information to match the study face using just the first two fixations, as evidenced by the plateau in their results in Figure 4. After this, subjects could continue to actively fixate the image or simply let their gaze wander while they considered and entered their response. Thus, perhaps many of the fixations recorded by the eye tracker in this condition were not actively being used by the

subjects to make their decision (were not task-relevant), which could explain why including them hampered NIMBLE's performance.

Discussion

Our Bayesian version of NIM provides several extensions to the original cognitive model (Lacroix et al., 2006). First, we recast NIM into a probabilistic framework, placing it on a firmer theoretical foundation. In this setting, NIM's spherical kernel becomes the likelihood function (a density estimator). We showed how this could be replaced by a more robust Gaussian kernel or by a nearest-neighbor density estimator. The resulting NIMBLE model demonstrates good performance on identification tasks for both faces and objects. We also showed that in face identification, the model's belief in the correct answer increases in a reasonable way as more evidence is gathered through further fixations, a property not enjoyed by the original NIM model's method of evidence combination.

In addition, we cast the problem of memory for faces as a classification problem, where we assume that faces from the study set are encoded with the context of the experiment (here, simply labeled as being from the study set). Our NIMBLE model demonstrates human levels of performance on a facial memory (familiar/unfamiliar) task. However, a more detailed examination of the relationship between NIMBLE and human processing revealed differences in both the apparent salience map, which is the front end of our model, and the memory component of the model when human fixations are used. These differences will require further refinements to the model in order to better match the human data.

One obvious difference is the methodology used in the two cases. Whereas the human subjects begin the experiment looking at a screen location off the face and saccade to the face, NIMBLE starts by computing a complete salience map from the entire full-resolution face image. A more reasonable paradigm might be for NIMBLE to also start off the face and compute the salience of the image using only the low-resolution information about the face that would be available from an object in the periphery. Clearly, the model would find the face salient and saccade to it. Before the first saccade, the representation of the face would be low resolution because it is out of the fovea, and so we hypothesize that the salience would be maximal near the center of the face (corresponding to human subjects first saccading to near the bridge of the nose). This idea also suggests potential future research to develop a more realistic salience model that computes salience based only on the currently available image information, rather than one computed on the entire image in parallel in advance (as is currently done).

The first-fixation performance discrepancy between the human subjects and NIMBLE may be due to the humans' imperfect perception of the studied face during a single fixation (the duration of the first fixation is 295 ms on average in the human experiment). Perhaps the current model moves its beliefs too far based on the current input, resulting in the high accuracy after the first fixation. Humans appear to be more "skeptical" in their updating until they have a second fixation. We could account for this using a generative model that is a mixture of noise and actual beliefs, as was done by Nelson and Cottrell (2007) to model the gradual acquisition of concepts in a learning task.

Alternatively, the discrepancy may also be due to task switching from localizing to exploring for recognition that occurs during the first fixation. Subjects begin by planning a localizing saccade from the center of the screen to the center of the stimulus (Renninger et al., 2007) and may not take in all of the information from this first fixation location that is required for recognition. Future work could test this hypothesis by instructing and/or restricting participants to make only one fixation during the face recognition task and increasing the preview time of the average face in the periphery to reduce the task-switching cost. Based on NIMBLE's results, our hypothesis is that this will improve the human subjects' performance in the one-fixation condition.

Similar to what we have proposed here, Lacroix et al. (2007) have developed an extension of their original NIM model, called NIM-CLASS, which can be applied to multi-class identification tasks by storing a class label with each memorized fragment. They assign a label to a new fragment by finding the peak in the histogram of its nearest neighbors' labels. However, the model is still heuristic rather than probabilistic. A further extension in NIM-CLASS that is beyond what we have done here is to include the influence of top-down attention by also storing the image coordinates of each memorized fragment as well as a low-resolution, global representation of the image that captures the gist of the image. Using this global representation, they direct future fixations to the area in the image that is most likely to reduce classification uncertainty. The computational complexity of this step makes it somewhat implausible for fixation planning. Bayesian methods exist for augmenting the salience calculation by including scene context (e.g., priors on target locations; Torralba, Oliva, Castelhano, & Henderson, 2006) and top-down influences (e.g., the likelihood of the features given the class; Zhang, Tong, Marks, Shan, & Cottrell, in press). Such models could easily be integrated into NIMBLE's probabilistic framework.

Future improvements to NIMBLE will include more detailed modeling of the retinal and lateral geniculate nucleus (LGN) transformation used to convert fixated image locations into features for the memory model. This will move from the oversimplified square patch samples of the Gabor filter responses to a properly foveated retina model with lower resolution samples from the periphery. In addition, we plan to improve the selection of fixation points by integrating learned, task-specific feedback to direct NIMBLE's "eye" movements to sample from image locations with top-down interest as well as bottom-up salience. Since NIMBLE is a fully probabilistic model, it will be straightforward to integrate these more complex systems into the existing model.

Conclusions

Using the NIM model (Lacroix et al., 2006) as our starting point, we developed NIMBLE, a biologically inspired, saccade-based Bayesian model of face and object recognition. We have demonstrated that NIMBLE's performance is comparable to human performance on standard identification and recognition memory tasks and that this biologically inspired model approaches the best machine vision results. In addition, the sequential sampling version of NIMBLE demonstrates that, like humans, our system can achieve correct identification and recognition of faces and objects after a very small number of fixations. Implementing NIMBLE using actual human fixations improves performance considerably,

suggesting that in a face recognition memory task, humans fixate locations that are optimally suited to solving the problem.

Acknowledgments

This work is supported by NIMH Grant MH57075 to GWC, a James S. McDonnell Foundation Grant to the Perceptual Expertise Network (Isabel Gauthier, PI), and NSF Grant #SBE-0542013 to the Temporal Dynamics of Learning Center (GWC, PI). LB was supported by an IGERT fellowship (NSF DGE-0333451 to GWC).

References

Belongie S, Malik J, & Puzicha J (2002). Shape matching and object recognition using shape contexts. Pattern Analysis and Machine Intelligence, 24–4, 509–522.

Bishop C (1995). Neural networks for pattern recognition. Oxford, UK: Oxford University Press.

Dailey M, Cottrell G, & Busey T (1998). Facial memory is kernel density estimation (almost) In Kearns MS, Solla SA, & Cohn DA (Eds.), Advances in neural information processing systems (vol. 11, pp. 24–30). Cambridge, MA: MIT Press.

Dailey MN, Cottrell GW, Padgett C, & Adolphs R (2002). EMPATH: A neural network that categorizes facial expressions. Journal of Cognitive Neuroscience, 14, 1158–1173. [PubMed: 12495523]

Dollar P, Rabaud V, Cottrell G, & Belongie S (2005). Behavior recognition via sparse spatio-temporal features. Proceedings of the Joint IEEE Workshop on Visual Surveillance & Performance Evaluation of Tracking & Surveillance.

Duchaine B, & Nakayama K (2005). Dissociations of face and object recognition in developmental prosopagnosia. Journal of Cognitive Neuroscience, 17, 249–261. [PubMed: 15811237]

Foulsham T, & Underwood G (2008). What can saliency models predict about eye movements? Spatial and sequential aspects of fixations during encoding and recognition. Journal of Vision, 8(2):6, 1–17, http://journalofvision.org/8/2/6/, doi:10.1167/8.2.6. [Article]

Henderson JM (2003). Human gaze control during real-world scene perception. Trends in Cognitive Science, 7, 498–504.

Henderson JM, Williams CC, & Falk RJ (2005). Eye movements are functional during face learning. Memory & Cognition, 33, 98–106.

Hintzman D (1984). MINERVA 2: A simulation model of human memory. Behavior Research Methods, Instruments and Computers, 16, 96–101.

Hsiao J, & Cottrell G (in press). Two fixations suffice in face recognition. Psychological Science.

Itti L, & Koch C (2001). Computational modelling of visual attention. Nature Reviews, Neuroscience, 2, 194–203. [PubMed: 11256080]

Jones JP, & Palmer LA (1987). An evaluation of the two-dimensional Gabor filter model of simple receptive fields in cat striate cortex. Journal of Neurophysiology, 58, 1233–1258. [PubMed: 3437332]

Kittler J, Hatef M, Duin R, & Matas J (1998). On combining classifiers. IEEE Transactions on Pattern Analysis and Machine Intelligence, 20, 226–239.

Lacroix J, Murre J, & Postma E (2006). Modeling recognition memory using the similarity structure of natural input. Cognitive Science, 30, 121–145. [PubMed: 21702811]

Lacroix J, Murre J, Postma E, & Van den Herik H (2004). The natural input memory model. Proceedings of the 26th Annual Meeting of the Cognitive Science Society.

Lacroix J, Postma E, & Van den Herik H (2007). Modeling visual classification using bottom-up and top-down fixation selection. Proceedings of the 29th Annual Meeting of the Cognitive Science Society.

Lowe D (2004). Distinctive image features from scale-invariant keypoints. International Journal of Computer Vision, 20, 91–110.

Mozer M, Shettel M, & Vecera S (2006). Top-down control of visual attention: A rational account In Weiss Y, Scholkopf B, & Platt J (Eds.), Advances in neural information processing systems, (vol. 18, pp. 923–930). Cambridge, MA: MIT Press.

Nelson J, & Cottrell G (2007). A probabilistic model of eye movements in concept formation. Neurocomputing, 70, 2256–2272. [PubMed: 22787288]

Nene S, Nayar SK, & Murase H (1996). Columbia object image library (COIL-100) (Tech. Rep.).

Nosofsky RM, & Palmeri TJ (1997). An exemplar-based random walk model of speeded classification. Psychological Review, 104, 266–300. [PubMed: 9127583]

Noton D, & Stark L (1971). Scanpaths in saccadic eye movements while viewing and recognizing patterns. Vision Research, 11, 929–942. [PubMed: 5133265]

Palmeri TJ, & Gauthier I (2004). Visual object understanding. Nature Reviews, Neuroscience, 5, 291–303. [PubMed: 15034554]

Phillips J, Wechsler H, Huang J, & Rauss P (1998). The FERET database and evaluation procedure for face-recognition algorithms. Image & Vision Computing, 16, 295–306.

Raaijmakers J, & Shiffrin R (2002). Models of memory In Pashler H & Medin D (Eds.), Stevens' handbook of experimental psychology (3rd ed., vol. 2), Memory and cognitive processes (pp. 43–76). Wiley.

Raj R, Geisler WS, Frazor RA, & Bovik AC (2005). Contrast statistics for foveated visual systems: Fixation selection by minimizing contrast entropy. Journal of the Optical Society of America A, Optics, Image Science, and Vision, 22, 2039–2049.

Renninger L, Coughlan J, Verghese P, & Malik J (2005). An information maximization model of eye movements In Saul LK, Weiss Y, & Bottou L (Eds.), Advances in neural information processing systems, (vol. 17, pp. 1121–1128). Cambridge, MA: MIT Press. [PubMed: 16175670]

Renninger LW, Verghese P, & Coughlan J (2007). Where to look next? Eye movements reduce local uncertainty. Journal of Vision, 7(3):6, 1–17, http://journalofvision.org/7/3/6/, doi:10.1167/7.3.6. [Article]

Tatler BW (2007). The central fixation bias in scene viewing: Selecting an optimal viewing position independently of motor biases and image feature distributions. Journal of Vision, 7(14):4, 1–17, http://journalofvision.org/7/14/4/, doi:10.1167/7.14.4. [Article]

Torralba A, Oliva A, Castelhano MS, & Henderson JM (2006). Contextual guidance of eye movements and attention in real-world scenes: The role of global features in object search. Psychological Review, 113, 766–786. [PubMed: 17014302]

Ullman S, Vidal-Naquet M, & Sali E (2002). Visual features of intermediate complexity and their use in classification. Nature Neuroscience, 5, 682–687. [PubMed: 12055634]

Wolfe J (1994). Guided search 2.0: A revised model of visual search. Psychonomic Bulletin & Review, 1, 202–238. [PubMed: 24203471]

Yamada K, & Cottrell G (1995). A model of scan paths applied to face recognition. Proceedings of the 17th Annual Cognitive Science Conference, 55–60.

Yarbus A (1967). Eye movements and vision. New York: Plenum Press.

Zelinsky G, Zhang W, Yu B, Chen X, & Samaras D (2006). The role of top-down and bottom-up processes in guiding eye movements during visual search In Weiss Y, Schölkopf B, & Platt J (Eds.), Advances in neural information processing systems (vol. 18, pp. 1569–1576). Cambridge, MA: MIT Press.

Zhang L, Tong M, Marks T, Shan H, & Cottrell G (in press). SUN: A Bayesian framework for saliency using natural statistics. Journal of Vision.

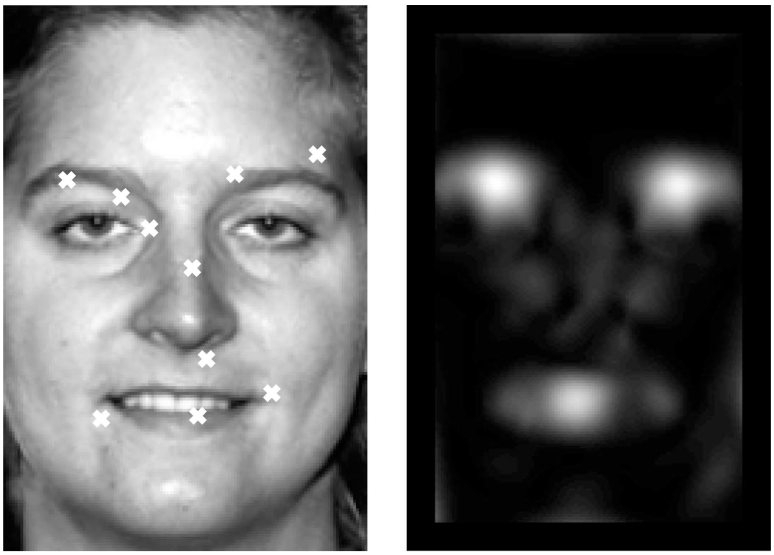

Figure 1.

(a) An image from the FERET database with 10 sample fixation points. (b) The corresponding salience map generated using the technique of Yamada and Cottrell (1995). The fixations shown in (a) were chosen randomly according to this salience map, and while they tend to cluster around highly salient areas, inhibition of return enforces a more even distribution of fixations across the image.

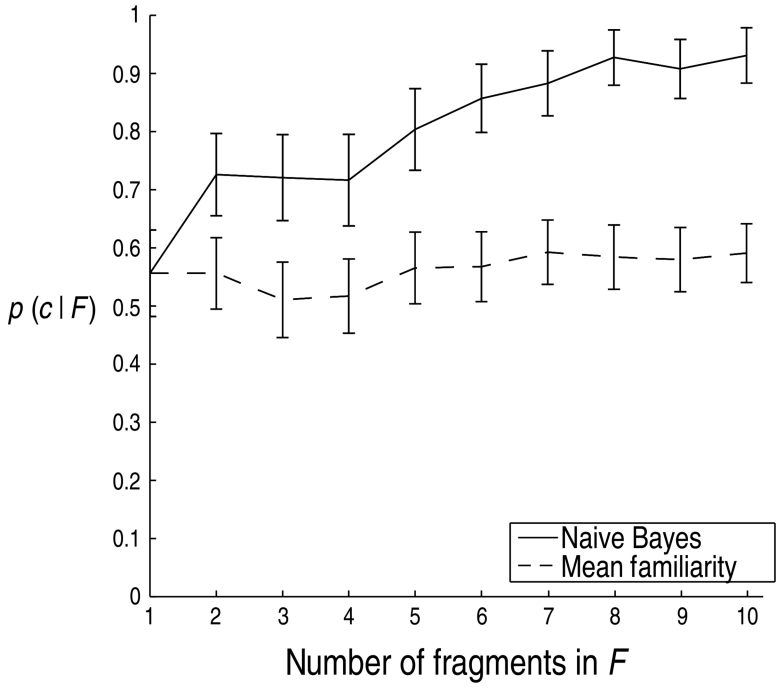

Figure 2.

NIMBLE's posterior probability of the *correct* face class vs. number of fixations in the 29-class face identification task. Posteriors are computed using both naive Bayes combination of fragment likelihoods (Equation 7) and mean familiarity combination of fragment likelihoods (Equation 8). The very low probabilities of the 28 incorrect classes are not shown.

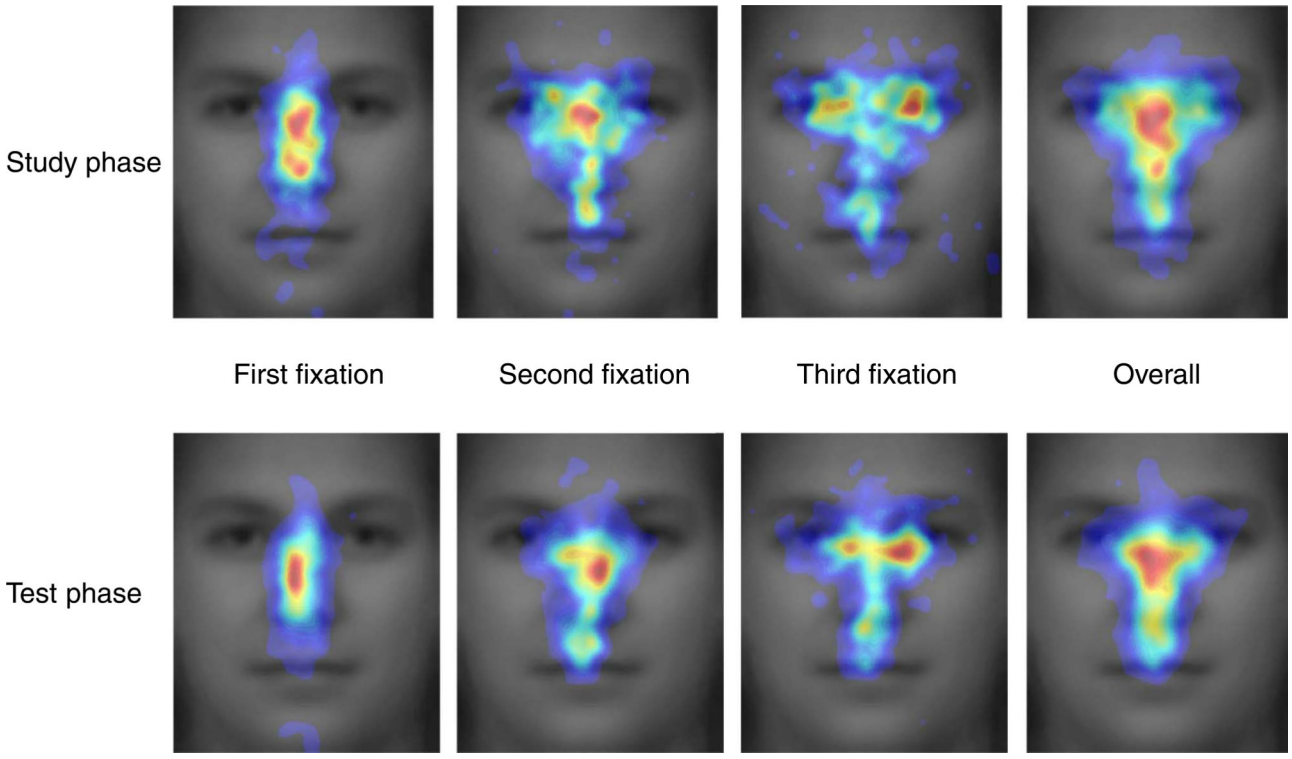

Figure 3.
Distribution of the first three fixations in all trials and overall fixations from all subjects during the study and the test phases (from Hsiao & Cottrell, in press).

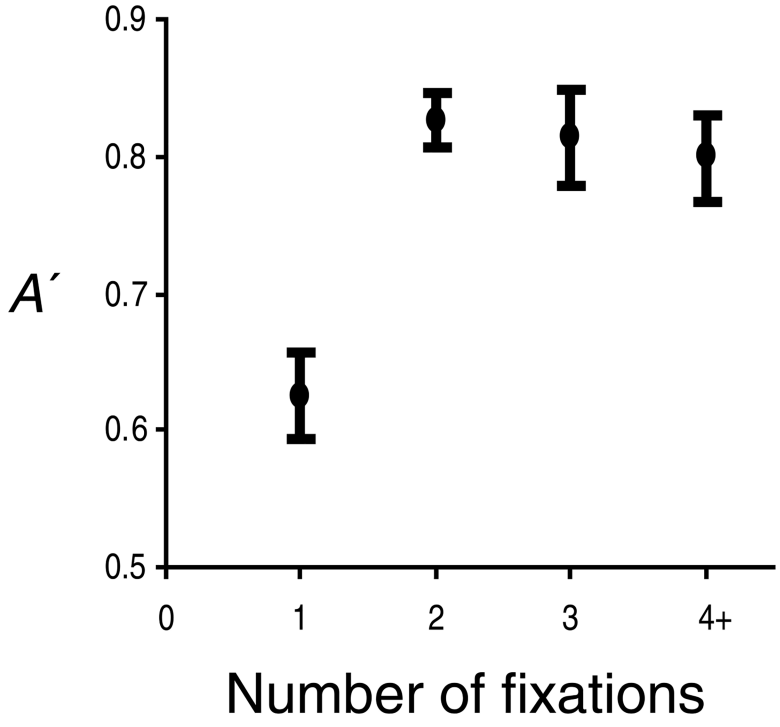

Figure 4.

Human participants' discrimination performance measured by A' in different fixation restriction conditions: one fixation, two fixations, three fixations, and the free viewing condition (4+). Error bars show standard errors.

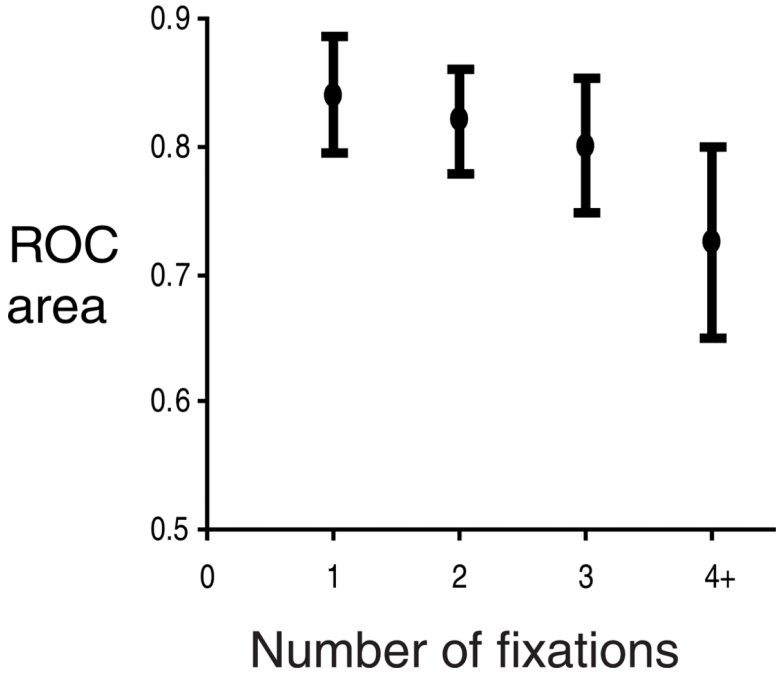

Figure 5.
NIMBLE's discrimination performance using human fixations, measured by ROC area in different fixation restriction conditions: one fixation, two fixations, three fixations, and the free viewing condition (4+ fixations). Error bars show standard errors.

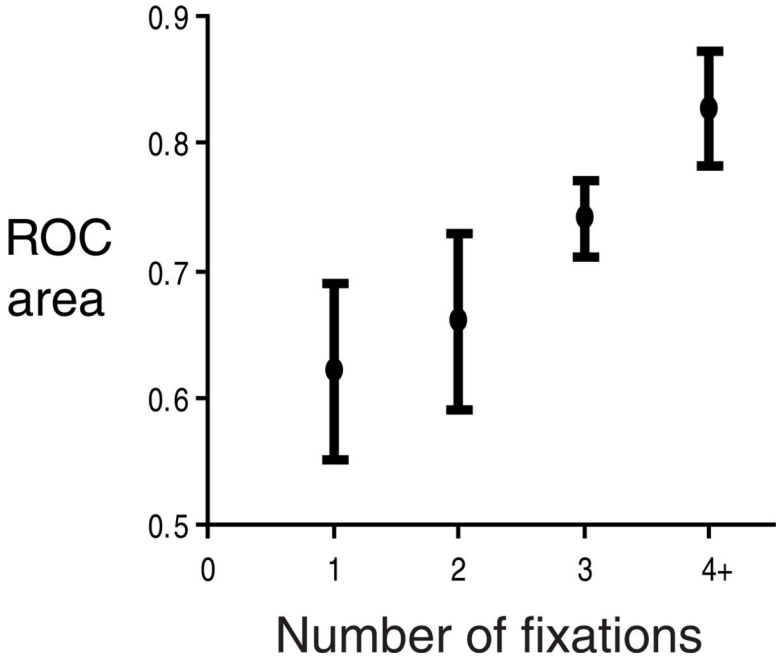

Figure 6.

NIMBLE's discrimination performance using the model of visual salience, measured by ROC area in different fixation restriction conditions: one fixation, two fixations, three fixations, and the average of 4 to 10 fixations (4+). Error bars show standard errors.

Table 1.

Model accuracy for NIMBLE identification memory tasks. Face ID uses 29 identities from FERET, Object ID uses 20 classes from COIL-100 (optimal Gaussian variance σ for object ID is 10 times greater than for face ID). Standard errors of the mean are computed over 5 random trials.

	Face ID accuracy (%)		Object ID accuracy (%)	
Kernel	**Naive Bayes**	**Mean familiarity**	**Naive Bayes**	**Mean familiarity**
Gaussian (σ = 1,10)	85.6 ±2	72.2 ± 2	87 ± 1	73.7 ± 2
kNN (k = 1)	89.2 ± 0.6	85.8 ±2	92.7 ±0.7	87 ± 0.4

J Vis. Author manuscript; available in PMC 2020 July 14.

Table 2.

Model ROC area for face recognition memory. Image likelihoods are determined by combining the familiarities of image fragments using either naive Bayes (Equation 7) or the mean of the fragment familiarities (Equation 8). The likelihood of an image given the distracter class is found using a background model with either 10 or 80 dimensions. Standard errors of the mean are computed over 5 random trials.

		ROC area	
Kernel	**Fragment combination**	**10-D BG**	**80-D BG**
Gaussian ($\sigma = 1$)	Naive Bayes	0.94 t 0.03	0.58 ± 0.02
	Mean familiarity	0.97 ± 0.02	0.62 ±0.13
kNN ($k = 1$)	Naive Bayes	0.93 ± 0.05	0.97 ± 0.02
	Mean familiarity	0.96 t 0.02	0.96 ±0.01